Digital Signal Processing 48 (2016) 349–360

Contents lists available at ScienceDirect

Digital Signal Processing

www.elsevier.com/locate/dsp

Multidimensional folding for sinusoidal order selection ☆

Kefei Liu [a], Lei Huang [b,*], Hing Cheung So [c], Jieping Ye [a]

[a] Department of Computational Medicine and Bioinformatics, University of Michigan, Ann Arbor, MI 48109, USA
[b] College of Information Engineering, Shenzhen University, Shenzhen 518060, China
[c] Department of Electronic Engineering, City University of Hong Kong, Hong Kong, China

ARTICLE INFO

Article history:
Available online 23 October 2015

Keywords:
Sinusoidal order selection
Harmonic retrieval
Multidimensional folding (MDF)
Estimation error (ESTER)
Shift invariance equality

ABSTRACT

Estimation of the number of harmonics in multidimensional sinusoids is studied in this paper. The ESTimation ERror (ESTER) is a subspace based detection approach that is robust against colored noise. However, the number of signals it can detect is very limited. To improve the identifiability, we propose to combine the multidimensional folding (MDF) techniques with ESTER for multidimensional sinusoidal order selection. Our algorithm development is inspired by the shift invariance properties of the two matrix slices resulting from multidimensional folding and unfolding, which have been exploited to extract the spatial frequencies in the literature. The maximum identifiable number of signals of the MDF-ESTER is of the order of magnitude of product of the lengths of all spatial dimensions with uniform spacing, which is significantly larger than that of the conventional multidimensional ESTER methods. Meanwhile, it inherits the robustness of the ESTER against colored noise, and performs comparably to state-of-the-art schemes when the number of signals is small.

1. Introduction

Multidimensional sinusoidal frequency estimation or harmonic retrieval (HR) [1] has numerous applications ranging from multiple-input multiple-output (MIMO) radar imaging [2], channel estimation in wireless communication systems [3–5] to nuclear magnetic resonance (NMR) spectroscopy [6,7]. Parametric approaches to N-dimensional (N-D) frequency estimation, e.g., N-D unitary estimation of signal parameters via rotational invariant techniques (ESPRIT) and its variants [8–11], N-D multiple signal classification (MUSIC) [12], multidimensional folding (MDF) [13,14], improved MDF [15], N-D rank reduction estimator (RARE) [16] and principal-singular-vector utilization for modal analysis (PUMA) [17,18] provide super-resolution estimation performance. However, they rely on the *a priori* knowledge of the number of signals, which is often unknown and must be estimated from the noisy multidimensional measurements. As a matter of fact, it is a challenge to accurately determine the number of complex sinusoids from noisy N-D data, because the noise is usually spatially color, thereby calling for development of robust methodologies for sinusoidal order estimation.

In matrix case, it is common to use the eigenvalue spectrum for detecting the number of signals. Classical eigenvalue based order selection rules include the information theoretic criterion based methods [19] such as minimum description length (MDL) [20] and Akaike information criterion (AIC) [21], which are optimal in the fixed dimension-length large sample-size asymptotic regime, and the random matrix theory (RMT) based algorithms [22–25] that are designed for large dimension-length but relatively small sample-size scenarios. All these algorithms rely on the assumption that the noise is independent and identically distributed (i.i.d.) Gaussian. For correlated noise environment, they generally suffer a performance degradation.

To handle colored-noise scenarios, a number of subspace based methods that exploit the eigenvectors have been proposed [26–30]. In [26,31], the ESTimation ERror (ESTER) has been proposed for detecting the number of complex sinusoids, namely, uniform harmonics. It utilizes the shift invariance property of the signal subspace spanned by the sinusoids. Later in [27], an improved version of ESTER called subspace based automatic model order selection (SAMOS) is developed by exploiting the singular values of the signal subspace matrix. Although with better performance, the number of identifiable signals of SAMOS is reduced by half compared with ESTER. Compared with the eigenvalue based methods, the subspace based methods are more robust against colored noise.

However, these methods do not have direct multilinear counterparts that correspond to the multidimensional sinusoidal order selection problem at hand. To handle that, in [32,33] the ESTER

☆ The work described in this paper was supported by the Natural Science Foundation of China (No. 61222106, 61171187).

* Corresponding author.
E-mail addresses: kefeil@umich.edu (K. Liu), lhuang@szu.edu.cn (L. Huang), hcso@ee.cityu.edu.hk (H.C. So), jpye@umich.edu (J. Ye).

http://dx.doi.org/10.1016/j.dsp.2015.10.001
1051-2004/

is extended to N-D case based on the higher-order singular value decomposition (HOSVD). By combining the shift invariance equalities of the sinusoidal signal subspace in all dimensions, the N-D ESTER provides an improvement over n-mode ESTER in probability of correct detection (PoD) as well as robustness against colored noise. However, the number of detectable signals is limited to the maximum spatial dimension length minus 2.

To improve the identifiability, we propose to apply the MDF techniques [13,14] combined with the ESTER criterion for multidimensional sinusoidal order selection. The idea of multidimensional folding is to extend an N-D tensor to a $(2N+1)$-D tensor and then nest the augmented tensor to a 3-D tensor (the length of the $(2N+1)$-th and third dimension are both equal to 2) by dimensionality embedding. The two matrix slices of the resultant 3-D tensor satisfy the shift invariance equation[1] based on which the spatial frequencies have been extracted [13,14]. In this work, we exploit the same shift invariance properties of the two matrix slices to estimate the sinusoidal order using the ESTER criterion.

The maximum identifiable number of signals of the MDF-ESTER is on the order of magnitude of $\prod_n I_n$, where n indexes the uniform-spacing spatial modes of the observation tensor, and I_n is the corresponding dimension length. This indicates a significant improvement over [32,33]. Meanwhile, it inherits the robustness of the ESTER against colored noise, and its performance is comparable to the existing N-D ESTER schemes [32,33] when the number of signals is small.

The remainder of this paper is organized as follows. In Section 2, we present the N-D HR data model. In Sections 3 and 4, our proposed algorithms with integration of multidimensional folding and ESTER for N-D sinusoidal order estimation are described. Section 3 is devoted to the single-snapshot case, while Section 4 addresses the multiple-snapshot case. Simulation results are provided in Section 5, and in Section 6, conclusions are drawn.

2. Data model

Tensor and matrix notation: In order to facilitate the distinction between scalars, matrices and tensors, the following notation is used: Scalars are denoted as italic letters $(a, b, \ldots, A, B, \ldots, \alpha, \beta, \ldots)$, column vectors as lower-case bold-face letters $(\boldsymbol{a}, \boldsymbol{b}, \ldots)$, matrices as bold-face capitals $(\boldsymbol{A}, \boldsymbol{B}, \ldots)$, and tensors as bold-face calligraphic letters $(\mathcal{A}, \mathcal{B}, \ldots)$. Lower-order parts are consistently named: the (i, j)-entry of a matrix $\boldsymbol{A}$ is denoted as $a_{i,j}$, and the (i, j, k)-entry of a third-order tensor $\mathcal{A}$ as $a_{i,j,k}$. The superscripts *, $^{\mathrm{T}}$, $^{\mathrm{H}}$ and † stand for complex conjugate, transpose, Hermitian transpose and Moore–Penrose pseudo inverse, respectively. The $\|\boldsymbol{A}\|_{\mathrm{F}}$ and $\|\boldsymbol{A}\|_2$ denote the Frobenius norm and spectral norm of $\boldsymbol{A}$, respectively. The $\sigma_{\max}(\boldsymbol{A})$ and $\sigma_{\min}(\boldsymbol{A})$ denote the largest singular value and smallest non-zero singular value of $\boldsymbol{A}$, respectively. We use $\diamond$ for the Khatri–Rao (column-wise Kronecker) product of two matrices with common number of columns, $\circ$ for the outer product, $\lceil\cdot\rceil$ for integer ceiling, and $\lfloor\cdot\rfloor$ for integer floor.

The tensor operations align with [35]: The n-mode vectors of a tensor $\mathcal{X} \in \mathbb{C}^{I_1 \times I_2 \times \cdots \times I_N}$ are obtained by varying the n-th index within its range $(1, \ldots, I_n)$ and keeping all other indices fixed. The n-mode product of $\mathcal{X}$ and $\boldsymbol{U} \in \mathbb{C}^{J_n \times I_n}$ along the n-th mode, denoted as $\mathcal{X} \times_n \boldsymbol{U} \in \mathbb{C}^{I_1 \times I_2 \cdots \times J_n \cdots \times I_N}$, is obtained by multiplying the n-mode vectors of $\mathcal{X}$ from the left-hand side by $\boldsymbol{U}$.

The noisy observations are modeled as a superposition of R damped/undamped N-D cisoids sampled on an N-D grid of size $I_1 \times \cdots \times I_N$ at T subsequent time instants:

$$x_{i_1,\ldots,i_N,t} = \sum_{r=1}^{R} s_r(t) \prod_{n=1}^{N} e^{(i_n-1)\left(\zeta_r^{(n)} + j\mu_r^{(n)}\right)} + n^{(\mathrm{c})}_{i_1,\ldots,i_N,t},$$
$$i_n = 1, 2, \ldots, I_n, n = 1, 2, \ldots, N,\ t = 1, 2, \ldots, T, \tag{1}$$

where $\mu_r^{(n)}$ and $\zeta_r^{(n)} \le 0$ denote respectively the frequency and damping factor of the i-th cisoid in the n-th mode. The cisoid is undamped when $\zeta_r^{(n)} = 0$ and damped when $\zeta_r^{(n)} < 0$. The $s_r(t)$ is the complex amplitude of the r-th cisoid at time instant t, and $n^{(\mathrm{c})}_{i_1,\ldots,i_N,t}$ models the additive colored noise component inherent in the measurement process [36–39]. Here, $T \ge 1$ is the number of snapshots in the temporal dimension, and $T = 1$ and $T > 1$ correspond to single-snapshot and multiple-snapshot N-D sinusoid models, respectively.

Denote

$$\boldsymbol{a}_r^{(n)} = \boldsymbol{a}\left(\zeta_r^{(n)} + j\mu_r^{(n)}\right) = \begin{bmatrix} 1 \\ e^{\zeta_r^{(n)} + j\mu_r^{(n)}} \\ \vdots \\ e^{(I_n-1)\left(\zeta_r^{(n)} + j\mu_r^{(n)}\right)} \end{bmatrix} \tag{2}$$

as the array steering vector of the i-th signal in the n-th mode, and $\boldsymbol{s}_r = [s_r(1), \ldots, s_r(T)]^{\mathrm{T}}$ as the amplitude vector of the i-th signal. In tensor form, (1) is expressed as

$$\mathcal{X} = \sum_{r=1}^{R} \boldsymbol{a}_r^{(1)} \circ \boldsymbol{a}_r^{(2)} \circ \cdots \circ \boldsymbol{a}_r^{(N)} \circ \boldsymbol{s}_r + \mathcal{N}^{(\mathrm{c})}, \tag{3}$$

where $\mathcal{X}$ and $\mathcal{N}^{(\mathrm{c})} \in \mathbb{C}^{I_1 \times \cdots \times I_N \times T}$ are the observation and noise tensors, respectively. In the absence of noise, $\mathcal{X}$ is a sum of R rank-one tensors (outer-product of vectors) [40] each of which corresponds to an N-D cisoid. Given the noisy measurement tensor $\mathcal{X}$, our goal is to estimate the number of cisoids R.

Let $\boldsymbol{A}^{(n)}$, $n = 1, 2, \ldots, N$, be the array steering matrix that collects all the array steering vectors in the n-th mode:

$$\boldsymbol{A}^{(n)} = \begin{bmatrix} \boldsymbol{a}_1^{(1)} & \cdots & \boldsymbol{a}_R^{(1)} \end{bmatrix} = \begin{bmatrix} 1 & \cdots & 1 \\ e^{\zeta_1^{(n)} + j\mu_1^{(n)}} & \cdots & e^{\zeta_R^{(n)} + j\mu_R^{(n)}} \\ \vdots & \ddots & \vdots \\ e^{(I_n-1)\left(\zeta_1^{(n)} + j\mu_1^{(n)}\right)} & \cdots & e^{(I_n-1)\left(\zeta_R^{(n)} + j\mu_R^{(n)}\right)} \end{bmatrix},$$

and $\boldsymbol{S} = [\boldsymbol{s}_1 \boldsymbol{s}_2 \ldots \boldsymbol{s}_R] \in \mathbb{C}^{T \times R}$ contains the complex amplitudes of R cisoids at all N samples. Using n-mode products, (3) can be rewritten as

$$\mathcal{X} = \mathcal{I}_{N+1,R} \times_1 \boldsymbol{A}^{(1)} \cdots \times_N \boldsymbol{A}^{(N)} \times_{N+1} \boldsymbol{S} + \mathcal{N}^{(\mathrm{c})}, \tag{4}$$

where $\mathcal{I}_{N+1,R}$ represents the N-D identity tensor of size $R \times R \cdots \times R$, whose elements are equal to one when $i_1 = i_2 = \cdots = i_{N+1}$ and zero otherwise.

It is worth noting that our proposed detection algorithm can be also applied in the partly uniform multidimensional HR model, where only part (but at least 1) of the factor matrices $\boldsymbol{A}^{(n)}$, $n = 1, 2, \ldots, N$, have a Vandermonde structure. Such a partly uniform multidimensional HR model may appear in array processing which employs a uniform linear or rectangular array at the transmitter while a non-uniform antenna array at the receiver, or an antenna array with uniform spacing along one array axis but non-uniform spacing along the other axis [1]. For the partly uniform multidimensional HR model, the (spatial) dimensions with a non-uniform structure are merged with the temporal dimension via block unfolding [41,42] so that the temporal dimension in (1) accounts for these non-exponential dimensions as well.

[1] For undamped (constant-modulus) sinusoidal model, instead of constructing an additional dimension of length 2, forward–backward averaging [34] is exploited to construct the shift invariance equation in [14].

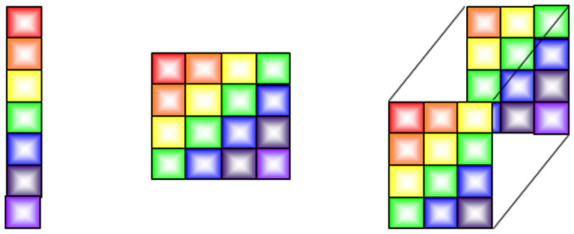

Fig. 1. Multidimensional folding of a 7×1 vector into a 4×4 matrix and a $4 \times 3 \times 2$ three-way array. Left: a vector of length $I_1 = 7$; middle: the resultant Hankel matrix of size $I_{1,1} \times I_{2,1}$ from multidimensional folding of the vector, with $I_{1,1} = I_{2,1} = 4$. The columns of the resultant matrix are generated by sliding a window of $I_{1,1}$ elements and with $(I_{1,1} - 1)$ overlapping elements between adjacent windows along the elements of the vector; right: the resultant three-way array of size $I_{1,1} \times I_{2,1} \times I_{\mathrm{SI},1}$ from multidimensional folding of the vector, with $I_{1,1} = 4$, $I_{2,1} = 3$, and $I_{\mathrm{SI},1} = 2$. The columns of each matrix slice of the resultant three-way array are generated by sliding a window of $I_{1,1}$ elements and with $(I_{1,1} - 1)$ overlapping elements between adjacent windows along the elements of the vector, and the two matrix slices are generated via an additional sliding window of length $(I_1 - 1)$ and of $(I_1 - 2)$ overlapping elements between adjacent windows along the elements of the vector. Note that both matrix slices in the right figure are of Hankel structures.

3. *N*-D sinusoidal order estimation using multidimensional folding: single-snapshot case

Consider the N-D damped/undamped sinusoidal model and denote $z_{r,n} = e^{\zeta_r^{(n)} + j\mu_r^{(n)}}$, $r = 1, 2, \ldots, R$, $n = 1, 2, \ldots, N$, hereafter for brevity in notation. For the single-snapshot ($T = 1$) case, $\mathcal{X}$ is N-D and the signals along all N dimensions are exponential cisoids. The $\mathcal{X}$ is extended/augmented and then folded into a $(2N+1)$-D tensor $\mathcal{X}^+$, in the same line as [13]:

$$x^+_{i_{1,1},i_{2,1},i_{1,2},i_{2,2},\ldots,i_{1,N},i_{2,N},i_{\mathrm{SI},1}} = x_{i_{1,1}+i_{2,1}+i_{\mathrm{SI},1}-2,i_{1,2}+i_{2,2}-1,\ldots,i_{1,N}+i_{2,N}-1}, \tag{5}$$

where $i_{1,n} = 1, 2, \ldots, I_{1,n}$, $i_{2,n} = 1, 2, \ldots, I_{2,n}$ for $n = 1, 2, \ldots, N$, and $i_{\mathrm{SI},1} = 1, 2$, with

$$I_{\mathrm{SI},1} = 2 \tag{6a}$$

$$I_{1,1} + I_{2,1} + I_{\mathrm{SI},1} = I_1 + 2 \tag{6b}$$

$$I_{1,n} + I_{2,n} = I_n + 1,\ n = 2, \ldots, N \tag{6c}$$

In (5), the 1-mode vectors of $\mathcal{X}$ of size $I_1 \times 1$ are arranged as a three-way array of size $I_{1,1} \times I_{2,1} \times I_{\mathrm{SI},1}$, and its n-mode vectors of size $I_n \times 1$, $n = 2, \ldots, N$, are arranged as a Hankel matrix (a square matrix with constant skew-diagonals) of size $I_{1,n} \times I_{2,n}$, as illustrated in Fig. 1. As will be clear later, the dimension indexed by $i_{\mathrm{SI},1}$ is used to construct the shift invariance equality.

In the absence of noise, $\mathcal{X}^+ \in \mathbb{C}^{I_{1,1} \times I_{2,1} \times I_{1,2} \times I_{2,2} \times \cdots \times I_{1,N} \times I_{2,N} \times I_{\mathrm{SI},1}}$ is represented in scalar form as

$$x^+_{i_{1,1},i_{2,1},i_{1,2},i_{2,2},\ldots,i_{1,N},i_{2,N},i_{\mathrm{SI},1}} = \sum_{r=1}^{R} s_r z_{r,1}^{i_{\mathrm{SI},1}-1} \prod_{n=1}^{N} z_{r,n}^{i_{1,n}-1} z_{r,n}^{i_{2,n}-1}, \tag{7}$$

and in tensor form as

$$\mathcal{X}^+ = \mathcal{D}_{2N+1,R} \times_1 \boldsymbol{A}_1^{(1)} \times_2 \boldsymbol{A}_2^{(1)} \cdots \times_{2N-1} \boldsymbol{A}_1^{(N)} \times_{2N} \boldsymbol{A}_2^{(N)} \times_{2N+1} \boldsymbol{A}_{\mathrm{SI}}^{(1)},$$

where $\mathcal{D}_{2N+1,R}$ represents the $(2N+1)$-D superdiagonal tensor of size $R \times R \cdots \times R$, whose elements are all zeros except that the i-th diagonal element is equal to s_r,

$$\boldsymbol{A}_1^{(n)} = \begin{bmatrix} 1 & 1 & \cdots & 1 \\ z_{1,n} & z_{2,n} & \cdots & z_{R,n} \\ \vdots & \vdots & \ddots & \vdots \\ z_{1,n}^{I_{1,n}-1} & z_{2,n}^{I_{1,n}-1} & \cdots & z_{R,n}^{I_{1,n}-1} \end{bmatrix} \in \mathbb{C}^{I_{1,n} \times R}, \tag{8}$$

$$\boldsymbol{A}_2^{(n)} = \begin{bmatrix} 1 & 1 & \cdots & 1 \\ z_{1,n} & z_{2,n} & \cdots & z_{R,n} \\ \vdots & \vdots & \ddots & \vdots \\ z_{1,n}^{I_{2,n}-1} & z_{2,n}^{I_{2,n}-1} & \cdots & z_{R,n}^{I_{2,n}-1} \end{bmatrix} \in \mathbb{C}^{I_{2,n} \times R} \tag{9}$$

for $n = 1, 2, \ldots, N$, and

$$\boldsymbol{A}_{\mathrm{SI}}^{(1)} = \begin{bmatrix} 1 & 1 & \cdots & 1 \\ z_{1,1} & z_{2,1} & \cdots & z_{R,1} \end{bmatrix} \in \mathbb{C}^{2 \times R}. \tag{10}$$

By merging/unfolding/collapsing the $1, 3, \ldots, 2N-1$ dimensions and $2, 4, \ldots, 2N$ dimensions of $\mathcal{X}^+$ into one dimension, respectively, in the same way as described in [13], we obtain

$$\overline{\mathcal{X}^+} = \mathcal{D}_{3,R} \times_1 \boldsymbol{A}_1 \times_2 \boldsymbol{A}_2 \times_3 \boldsymbol{A}_{\mathrm{SI}}^{(1)}, \tag{11}$$

where

$$\boldsymbol{A}_1 = \boldsymbol{A}_1^{(N)} \diamond \boldsymbol{A}_1^{(N-1)} \diamond \cdots \diamond \boldsymbol{A}_1^{(1)} \in \mathbb{C}^{I_{1,1} I_{1,2} \cdots I_{1,N} \times R}, \tag{12}$$

$$\boldsymbol{A}_2 = \boldsymbol{A}_2^{(N)} \diamond \boldsymbol{A}_2^{(N-1)} \diamond \cdots \diamond \boldsymbol{A}_2^{(1)} \in \mathbb{C}^{I_{2,1} I_{2,2} \cdots I_{2,N} \times R}. \tag{13}$$

The two matrix slices of $\overline{\mathcal{X}^+}$ along the third dimension are [40]

$$\boldsymbol{X}_1^+ = \boldsymbol{A}_1 \operatorname{diag}\{\boldsymbol{s}\} \boldsymbol{A}_2^{\mathrm{T}} \in \mathbb{C}^{I_{1,1} I_{1,2} \cdots I_{1,N} \times I_{2,1} I_{2,2} \cdots I_{2,N}} \tag{14}$$

$$\boldsymbol{X}_2^+ = \boldsymbol{A}_1 \boldsymbol{\Phi}^{(1)} \operatorname{diag}\{\boldsymbol{s}\} \boldsymbol{A}_2^{\mathrm{T}} \in \mathbb{C}^{I_{1,1} I_{1,2} \cdots I_{1,N} \times I_{2,1} I_{2,2} \cdots I_{2,N}} \tag{15}$$

where

$$\boldsymbol{s} = \begin{bmatrix} s_1 & s_2 & \cdots & s_R \end{bmatrix} \tag{16}$$

$$\boldsymbol{\Phi}^{(1)} = \operatorname{diag}\left\{\begin{bmatrix} z_{1,1} & z_{2,1} & \cdots & z_{R,1} \end{bmatrix}\right\}. \tag{17}$$

Fig. 2 illustrates the multidimensional folding/unfolding process for a two-way tensor (i.e., matrix) of size 7×4, where $I_{1,1} = 4$, $I_{2,1} = 3$, $I_{1,2} = 2$, and $I_{2,2} = 3$.

Since $\boldsymbol{A}_1$ and $\boldsymbol{A}_2$ are the Khatri–Rao products of N Vandermonde matrices, according to Proposition 4 of [13], when

$$R \leq \min(I_{1,1} I_{1,2} \cdots I_{1,N}, I_{2,1} I_{2,2} \cdots I_{2,N}), \tag{18}$$

both $\boldsymbol{A}_1$ and $\boldsymbol{A}_2$ are almost surely (a.s.) of full rank R. Therefore, $\boldsymbol{X}_1^+$, $\boldsymbol{X}_2^+$ and hence

$$\boldsymbol{X}^+ = \begin{bmatrix} \boldsymbol{X}_1^+ \\ \boldsymbol{X}_2^+ \end{bmatrix} = \begin{bmatrix} \boldsymbol{A}_1 \\ \boldsymbol{A}_1 \boldsymbol{\Phi}^{(1)} \end{bmatrix} \operatorname{diag}\{\boldsymbol{s}\} \boldsymbol{A}_2^{\mathrm{T}} \tag{19}$$

have rank R. On the other hand, by applying the singular value decomposition on $\boldsymbol{X}^+$, we obtain

$$\boldsymbol{X}^+ = \boldsymbol{U} \boldsymbol{\Lambda} \boldsymbol{V}^{\mathrm{H}} \tag{20}$$

where

$$\boldsymbol{U} \in \mathbb{C}^{2I_{1,1} I_{1,2} \cdots I_{1,N} \times 2I_{1,1} I_{1,2} \cdots I_{1,N}} \text{ and } \boldsymbol{V} \in \mathbb{C}^{I_{2,1} I_{2,2} \cdots I_{2,N} \times I_{2,1} I_{2,2} \cdots I_{2,N}}$$

are unitary matrices containing the left and right singular vectors, respectively, and $\boldsymbol{\Lambda}$ is a diagonal matrix collecting the singular values sorted in descending order. Let

$$\boldsymbol{U}_r = \begin{bmatrix} \boldsymbol{U}_{r,1} \\ \boldsymbol{U}_{r,2} \end{bmatrix} \tag{21}$$

collect the r leftmost columns of $\boldsymbol{U}$. From the comparison between (19) and (20), it follows that in the absence of noise,

$$\boldsymbol{U}_R = \begin{bmatrix} \boldsymbol{U}_{R,1} \\ \boldsymbol{U}_{R,2} \end{bmatrix} \quad \text{and} \quad \begin{bmatrix} \boldsymbol{A}_1 \\ \boldsymbol{A}_1 \boldsymbol{\Phi}^{(1)} \end{bmatrix} \tag{22}$$

span the same subspace. Therefore, there exists a non-singular matrix $\boldsymbol{T} \in \mathbb{C}^{R \times R}$ such that

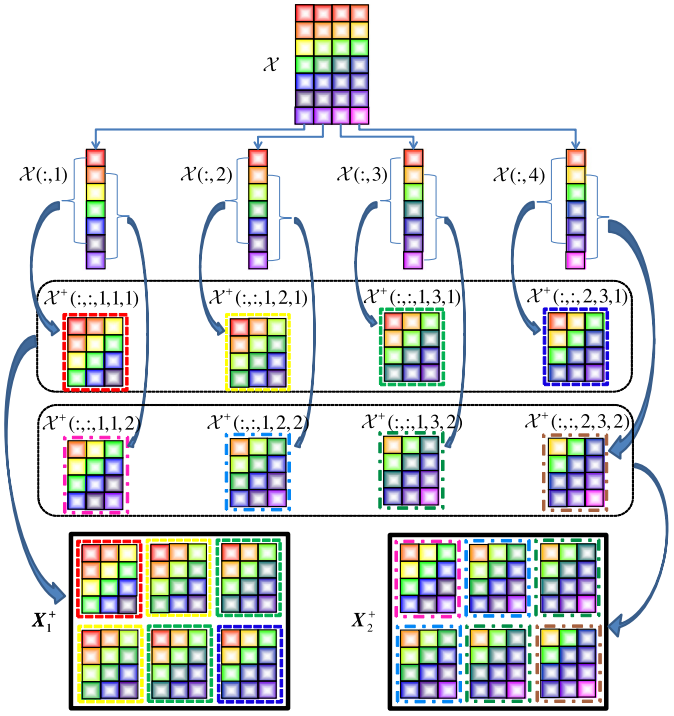

Fig. 2. Multidimensional folding/unfolding of a two-way tensor (i.e., matrix) $\mathcal{X}$ of size 7×4. From top to bottom: (i) $\mathcal{X}$; (ii) columns of $\mathcal{X}$ (note that the color sets used for embodying the elements of different columns are different, although the difference is subtle); (iii) augmented 5-D tensor $\mathcal{X}^+$. The eight boxes with dashed borders in the two rectangles with round corners correspond to the matrix slices of $\mathcal{X}^+$. Note that the matrix slices $\mathcal{X}^+(:,:,2,1,1)$ and $\mathcal{X}^+(:,:,2,2,1)$ are not shown here due to the space limit and they are equal to $\mathcal{X}^+(:,:,1,2,1)$ and $\mathcal{X}^+(:,:,1,3,1)$, respectively, according to (5). Likewise, since $\mathcal{X}^+(:,:,2,1,2)$ and $\mathcal{X}^+(:,:,2,2,2)$ are equal to $\mathcal{X}^+(:,:,1,2,2)$ and $\mathcal{X}^+(:,:,1,3,2)$, respectively, they are not shown as well; (iv) the obtained $\overline{\mathcal{X}^+}$ of size $8 \times 9 \times 2$ after unfolding of $\mathcal{X}^+$, represented in its two matrix slices.

$$\begin{bmatrix} \boldsymbol{A}_1 \\ \boldsymbol{A}_1\boldsymbol{\Phi}^{(1)} \end{bmatrix} = \begin{bmatrix} \boldsymbol{U}_{R,1} \\ \boldsymbol{U}_{R,2} \end{bmatrix} \boldsymbol{T}. \tag{23}$$

It follows that

$$\boldsymbol{A}_1 = \boldsymbol{U}_{R,1}\boldsymbol{T}, \quad \boldsymbol{A}_1\boldsymbol{\Phi}^{(1)} = \boldsymbol{U}_{R,2}\boldsymbol{T}, \tag{24}$$

and hence there exists $\boldsymbol{\Psi}_R = \boldsymbol{U}_{R,1}^{\dagger}\boldsymbol{U}_{R,2} = \boldsymbol{T}\boldsymbol{\Phi}^{(1)}\boldsymbol{T}^{-1}$ such that

$$\boldsymbol{U}_{R,1}\boldsymbol{\Psi}_R = \boldsymbol{U}_{R,2}. \tag{25}$$

Equation (25) is called the shift or rotational invariance equation. The shift invariance property of the sinusoidal signal model has been used by ESPRIT [43] to estimate the frequencies.

3.1. Order selection based on estimation error

The ESTER [26,31] selects an appropriate model order based on the rotational invariance property of the signal subspace spanned by the sinusoids. It was derived by minimizing the error bound induced by passing an under-estimated model order to ESPRIT [43]. In this subsection, we will provide a brief derivation of ESTER based on the new shift invariance equation (25) obtained from MDF.

Define

$$\boldsymbol{E}_r = \boldsymbol{U}_{r,1}\boldsymbol{\Psi}_r - \boldsymbol{U}_{r,2}, \text{ with } \boldsymbol{\Psi}_r = \boldsymbol{U}_{r,1}^{\dagger}\boldsymbol{U}_{r,2}. \tag{26}$$

In case that $r < R$, the shift invariance equation (25) is not satisfied, and we have the following theorem.

Theorem 3.1. *In the absence of noise, for each eigenvalue $\hat{z}$ of $\boldsymbol{\Psi}_r$, there exists an eigenvalue z_r of $\boldsymbol{\Psi}_R = \boldsymbol{U}_{R,1}^{\dagger}\boldsymbol{U}_{R,2}$ such that*

$$\left|\hat{z} - z_r\right| \le \kappa_2 \left\|\boldsymbol{U}_{r,1}\boldsymbol{\Psi}_r - \boldsymbol{U}_{r,2}\right\|_2 \tag{27}$$

where

$$\kappa_2 = \frac{\sigma_{\max}\left(\begin{bmatrix} \boldsymbol{A}_1 \\ \boldsymbol{A}_1\boldsymbol{\Phi}^{(1)} \end{bmatrix}\right)}{\sigma_{\min}(\boldsymbol{A}_1)}. \tag{28}$$

Proof. The result can be obtained using the similar derivation process of [26]. For ease of reference, the proof is provided in Appendix A. □

When $1 \le r < R$, Theorem 3.1 indicates that the estimation error $\|\boldsymbol{E}_r\|_2 > 0$. This is because the eigenvalues of $\boldsymbol{\Psi}_R = \boldsymbol{T}\boldsymbol{\Phi}^{(1)}\boldsymbol{T}^{-1}$ and $\boldsymbol{\Phi}^{(1)}$ share the same set of eigenvalues $\{z_{1,1}, z_{2,1}, \ldots, z_{R,1}\}$, namely, the set of cisoids in the first mode, while in general $\hat{z} \notin \{z_{1,1}, z_{2,1}, \ldots, z_{R,1}\}$ and thus $\left|\hat{z} - z_r\right| > 0$. On the other hand, when $r > R$, it also holds that $\|\boldsymbol{E}_r\|_2 > 0$ since the noise eigenvectors do not satisfy the shift invariance property[2] [26].

Therefore, the minimum of zero of $\|\boldsymbol{E}_r\|_2$ is reached only at $r = R$. In practice, noise is present, and the estimated signal number, denoted by $\hat{R}_{\text{MDF-ESTER}}$, is obtained by minimizing the residual error:

$$\hat{R}_{\text{MDF-ESTER}} = \underset{r=1,2,\ldots,R_{\max}}{\arg\min} \left\|\boldsymbol{U}_{r,1}\boldsymbol{\Psi}_r - \boldsymbol{U}_{r,2}\right\|_2^2, \tag{29}$$

where $R_{\max}$ is the largest possible number of detectable cisoids and is stipulated by (18).

To maximize the number of detectable cisoids, $I_{1,n}$ and $I_{2,n}$, $n = 1, 2, \ldots, N$, are chosen according to (6) and (18) as

$$\begin{cases} \text{if } I_1 \text{ is even} & I_{1,1} = I_{2,1} = I_1/2 \\ \text{if } I_1 \text{ is old} & I_{1,1} = \frac{I_1-1}{2},\ I_{2,1} = \frac{I_1+1}{2}, \end{cases} \tag{30}$$

and for $n = 2, \ldots, N$,

$$\begin{cases} \text{if } I_n \text{ is even} & I_{1,n} = \frac{I_n}{2},\ I_{2,n} = \frac{I_n+2}{2} \\ \text{if } I_n \text{ is old} & I_{1,n} = I_{2,n} = \frac{I_n+1}{2}. \end{cases} \tag{31}$$

As a result, the maximum number of detectable cisoids is[3]

$$R_{\max} = \left\lfloor \frac{I_1}{2} \right\rfloor \prod_{n=2}^{N} \left\lceil \frac{I_n}{2} \right\rceil - 1 \tag{32}$$

3.2. Constant-envelope (undamped) HR case

For the constant-modulus (i.e., $\zeta_r^{(n)} = 0$) sinusoidal model, forward–backward averaging (FBA) [34] can be exploited. In addition to bringing a performance improvement (cf. Section 5), the incorporation of FBA yields a pair of matrices that satisfy the shift invariance equality, thus avoiding the need to construct the additional length-2 dimension indexed by $i_{\text{SI},1}$, as shown below.

The N-D noisy signal $\mathcal{X}$ is folded (extended) into a $2N$-D tensor [14]:

[2] Let $\boldsymbol{P}(r) = \boldsymbol{I}_{I_{1,1}I_{1,2}\cdots I_{1,N}} - \boldsymbol{U}_{r,1}\boldsymbol{U}_{r,1}^{\dagger}$ be the projector onto the orthogonal complement of $\mathfrak{N}(\boldsymbol{U}_{r,1})$. If $r > R$, $\mathfrak{N}(\boldsymbol{U}_{R,2}) = \mathfrak{N}(\boldsymbol{U}_{R,1}) \subset \mathfrak{N}(\boldsymbol{U}_{r,1})$, therefore $\boldsymbol{P}(r)\boldsymbol{U}_{R,2} = \boldsymbol{0}_{I_{1,1}I_{1,2}\cdots I_{1,N} \times R}$. Since $\boldsymbol{E}_r = \boldsymbol{P}(r)\boldsymbol{U}_{r,2}$, the R left columns of $\boldsymbol{E}_r$ are zero. However, the $(r-R)$ right columns of $\boldsymbol{E}_r$ do not belong to $\mathfrak{N}(\boldsymbol{U}_{r,1})$ in the general case, therefore the $(r-R)$ right columns of $\boldsymbol{E}_r$ are non-zero, and the error bound is positive.

[3] Note that in addition to $r = R$, the shift invariance equation (25) is also always satisfied when $r = I_{1,1}I_{1,2}\cdots I_{1,N}$ in which case $\boldsymbol{U}_{r,1}$ and $\boldsymbol{U}_{r,2}$ are both square matrices. To exclude this trivial case so that the number of signals R can be correctly detected, we assume that the candidate value $r \le I_{1,1}I_{1,2}\cdots I_{1,N} - 1$.

$$x^{+}_{i_{1,1},i_{2,1},i_{1,2},i_{2,2},\ldots,i_{1,N},i_{2,N}} = x_{i_{1,1}+i_{2,1}-1,i_{1,2}+i_{2,2}-1,\ldots,i_{1,N}+i_{2,N}-1}, \tag{33}$$

where $i_{1,n} = 1, 2, \ldots, I_{1,n}$, $i_{2,n} = 1, 2, \ldots, I_{2,n}$, with

$$I_{1,n} + I_{2,n} = I_n + 1,\ n = 1, 2, \ldots, N \tag{34}$$

In the absence of noise, the scalar and tensor representations of the resultant $2N$-D tensor $\mathcal{X}^{+}$ are respectively

$$x^{+}_{i_{1,1},i_{2,1},i_{1,2},i_{2,2},\ldots,i_{1,N},i_{2,N}} = \sum_{r=1}^{R} s_r \prod_{n=1}^{N} e^{j(i_{1,n}-1)\mu_r^{(n)}} e^{j(i_{2,n}-1)\mu_r^{(n)}},$$

and

$$\mathcal{X}^{+} = \mathcal{D}_{2N,R} \times_1 \boldsymbol{A}_1^{(1)} \times_2 \boldsymbol{A}_2^{(1)} \cdots \times_{2N-1} \boldsymbol{A}_1^{(N)} \times_{2N} \boldsymbol{A}_2^{(N)},$$

where

$$\boldsymbol{A}_1^{(n)} = \begin{bmatrix} 1 & 1 & \cdots & 1 \\ e^{j\mu_1^{(n)}} & e^{j\mu_2^{(n)}} & \cdots & e^{j\mu_R^{(n)}} \\ \vdots & \vdots & \ddots & \vdots \\ e^{j(I_{1,n}-1)\mu_1^{(n)}} & e^{j(I_{1,n}-1)\mu_2^{(n)}} & \cdots & e^{j(I_{1,n}-1)\mu_R^{(n)}} \end{bmatrix}$$

$$\boldsymbol{A}_2^{(n)} = \begin{bmatrix} 1 & 1 & \cdots & 1 \\ e^{j\mu_1^{(n)}} & e^{j\mu_2^{(n)}} & \cdots & e^{j\mu_R^{(n)}} \\ \vdots & \vdots & \ddots & \vdots \\ e^{j(I_{2,n}-1)\mu_1^{(n)}} & e^{j(I_{2,n}-1)\mu_2^{(n)}} & \cdots & e^{j(I_{2,n}-1)\mu_R^{(n)}} \end{bmatrix}.$$

By merging/unfolding/collapsing the $1, 3, \ldots, 2N-1$ dimensions and $2, 4, \ldots, 2N$ dimensions of $\mathcal{X}^{+}$ into one dimension, respectively, along the same line as [14], we obtain

$$\boldsymbol{X}^{+} = \boldsymbol{A}_1 \operatorname{diag}\{\boldsymbol{s}\} \boldsymbol{A}_2^{\mathrm{T}}, \tag{35}$$

where

$$\boldsymbol{A}_b = \boldsymbol{A}_b^{(N)} \diamond \boldsymbol{A}_b^{(N-1)} \diamond \cdots \diamond \boldsymbol{A}_b^{(1)} \in \mathbb{C}^{I_{b,1}\ldots I_{b,N} \times R}, b = 1, 2 \tag{36}$$

Next, we apply conjugation and then sequential rotations of 180 degrees of the entries of $\mathcal{X}$ along individual dimensions to obtain a new tensor $\mathcal{Y}$:

$$\mathcal{Y} \doteq \mathcal{X}^{*} \times_1 \boldsymbol{\Pi}_{I_1} \cdots \times_N \boldsymbol{\Pi}_{I_N}, \tag{37}$$

where $\boldsymbol{\Pi}_{I_n}$ denotes the $I_n \times I_n$ exchange matrix having ones on its antidiagonal and zeros elsewhere.

In the absence of noise, the entries of $\mathcal{Y}$ can be shown to be

$$y_{i_1,\ldots,i_N} \doteq x^{*}_{I_1+1-i_1,\ldots,I_N+1-i_N} = \sum_{r=1}^{R} \tilde{s}_r \prod_{n=1}^{N} e^{j(i_n-1)\mu_r^{(n)}},$$
$$i_n = 1, 2, \ldots, I_n, n = 1, 2, \ldots, N, \tag{38}$$

where $\tilde{s}_r = s_r^{*} \prod_{n=1}^{N} e^{-j(I_n-1)\mu_r^{(n)}}$. We see that $\mathcal{Y}$ contains the same cisoids as $\mathcal{X}$.

Following the same procedure as in the construction of $\mathcal{X}^{+}$ from $\mathcal{X}$, we can construct a matrix from $\mathcal{Y}$ as

$$\boldsymbol{Y}^{+} = \boldsymbol{A}_1 \operatorname{diag}\{\tilde{\boldsymbol{s}}\} \boldsymbol{A}_2^{\mathrm{T}} \in \mathbb{C}^{I_{1,1}I_{1,2}\cdots I_{1,N} \times I_{2,1}I_{2,2}\cdots I_{2,N}}, \tag{39}$$

where $\tilde{\boldsymbol{s}} = \begin{bmatrix} \tilde{s}_1 & \tilde{s}_2 & \cdots & \tilde{s}_R \end{bmatrix}$.

Figs. 3 and 4 respectively illustrate the forward and backward parts of the folding/unfolding process for a two-way tensor (i.e., matrix) of size 7×4, where $I_{1,1} = I_{2,1} = 4$, $I_{1,2} = 2$, and $I_{2,2} = 3$.

According to Proposition 4 of [13], when

$$R \le \min\left(I_{1,1}I_{1,2}\cdots I_{1,N}, I_{2,1}I_{2,2}\cdots I_{2,N}\right), \tag{40}$$

both $\boldsymbol{A}_1$ and $\boldsymbol{A}_2$ are a.s. full column rank R. Therefore, $\boldsymbol{X}^{+}$ and $\boldsymbol{Y}^{+}$ have full column rank R. Let

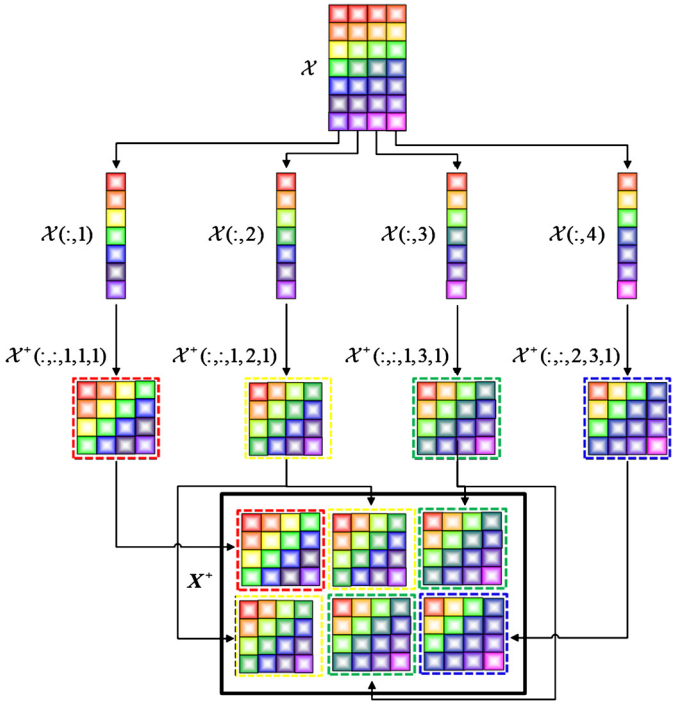

Fig. 3. Constant-modulus HR model: multidimensional folding/unfolding of the original two-way tensor (i.e., matrix) $\mathcal{X}$ of size 7×4 (forward part), with $I_{1,1} = I_{2,1} = 4$, $I_{1,2} = 2$, and $I_{2,2} = 3$. From top to bottom: (i) $\mathcal{X}$; (ii) columns of $\mathcal{X}$; (iii) augmented 5-D tensor $\mathcal{X}^{+}$ of size $4 \times 4 \times 2 \times 3 \times 2$. The four boxes with dashed borders of various colors correspond to the matrix slices of $\mathcal{X}^{+}$. Note that the matrix slices $\mathcal{Y}^{+}(:,:,2,1,1)$ and $\mathcal{Y}^{+}(:,:,2,2,1)$ are not shown here due to the space limit and they are equal to $\mathcal{X}^{+}(:,:,1,2,1)$ and $\mathcal{X}^{+}(:,:,1,3,1)$, respectively, according to (33); (iv) the obtained $\boldsymbol{X}^{+}$ of size 8×12 after unfolding of $\mathcal{X}^{+}$.

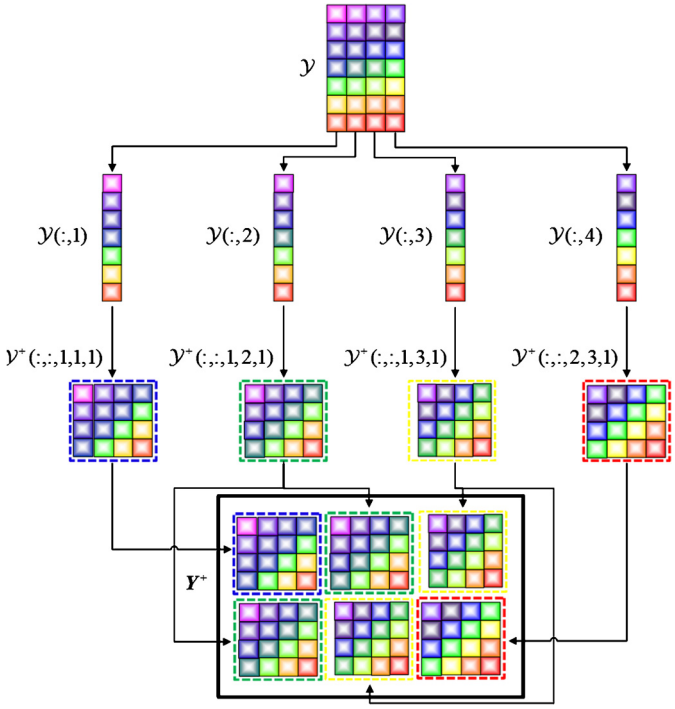

Fig. 4. Constant-modulus HR model: multidimensional folding/unfolding of the constructed (according to (39)) two-way tensor (i.e., matrix) $\mathcal{Y}$ of size 7×4 (backward part), with $I_{1,1} = I_{2,1} = 4$, $I_{1,2} = 2$, and $I_{2,2} = 3$. From top to bottom: (i) $\mathcal{Y}$; (ii) columns of $\mathcal{Y}$; (iii) augmented 5-D tensor $\mathcal{Y}^{+}$ of size $4 \times 4 \times 2 \times 3 \times 2$. The four boxes with dashed borders of various colors correspond to the matrix slices of $\mathcal{Y}^{+}$. Note that the matrix slices $\mathcal{Y}^{+}(:,:,2,1,1)$ and $\mathcal{Y}^{+}(:,:,2,2,1)$ are not shown here due to the space limit and they are equal to $\mathcal{Y}^{+}(:,:,1,2,1)$ and $\mathcal{Y}^{+}(:,:,1,3,1)$, respectively; (iv) the obtained $\boldsymbol{Y}^{+}$ of size 8×12 after unfolding of $\mathcal{Y}^{+}$.

$$\boldsymbol{U}_r = \begin{bmatrix} \boldsymbol{U}_{r,1} \\ \boldsymbol{U}_{r,2} \end{bmatrix} \tag{41}$$

with $\boldsymbol{U}_{r,1}, \boldsymbol{U}_{r,2} \in \mathbb{C}^{I_{1,1}I_{1,2}\cdots I_{1,N}\times R}$, collect the r left singular vectors associated with the r largest singular values of

$$\begin{bmatrix} \boldsymbol{X}^+ \\ \boldsymbol{Y}^+ \end{bmatrix} = \begin{bmatrix} \boldsymbol{A}_1 \operatorname{diag}\{\boldsymbol{s}\} \\ \boldsymbol{A}_1 \operatorname{diag}\{\tilde{\boldsymbol{s}}\} \end{bmatrix} \boldsymbol{A}_2^{\mathrm{T}}. \tag{42}$$

In the absence of noise, there exists a non-singular matrix $\boldsymbol{T} \in \mathbb{C}^{R\times R}$ such that

$$\begin{bmatrix} \boldsymbol{A}_1 \operatorname{diag}\{\boldsymbol{s}\} \\ \boldsymbol{A}_1 \operatorname{diag}\{\tilde{\boldsymbol{s}}\} \end{bmatrix} = \boldsymbol{U}_R \boldsymbol{T} = \begin{bmatrix} \boldsymbol{U}_{R,1} \\ \boldsymbol{U}_{R,2} \end{bmatrix} \boldsymbol{T}. \tag{43}$$

From (43), it follows that $\boldsymbol{A}_1 \operatorname{diag}\{\boldsymbol{s}\} = \boldsymbol{U}_{R,1}\boldsymbol{T}$, $\boldsymbol{A}_1 \operatorname{diag}\{\tilde{\boldsymbol{s}}\} = \boldsymbol{U}_{R,2}\boldsymbol{T}$, and hence

$$\boldsymbol{U}_{R,1}\boldsymbol{\Psi}_R = \boldsymbol{U}_{R,2} \tag{44}$$

where $\boldsymbol{\Psi}_R = \boldsymbol{T}\,(\operatorname{diag}\{\boldsymbol{s}\})^{-1} \operatorname{diag}\{\tilde{\boldsymbol{s}}\}\,\boldsymbol{T}^{-1}$.

In a similar manner of Section 3.1, it can be shown that in the absence of noise, $\|\boldsymbol{U}_{r,1}\boldsymbol{\Psi}_r - \boldsymbol{U}_{r,2}\|_2 > 0$ when $r \neq R$. In particular, for $r < R$, $\|\boldsymbol{U}_{r,1}\boldsymbol{\Psi}_r - \boldsymbol{U}_{r,2}\|_2$ is lower bounded by the absolute difference between an eigenvalue $\hat{z}$ of $\boldsymbol{\Psi}_r = \boldsymbol{U}_{r,1}^{\dagger}\boldsymbol{U}_{r,2}$ and its closest eigenvalue

$$z_r \in \{s_1^*/s_1 \prod_{n=1}^{N} e^{-j(I_n-1)\mu_1^{(n)}}, \ldots, s_R^*/s_R \prod_{n=1}^{N} e^{-j(I_n-1)\mu_R^{(n)}}\}$$

of $\boldsymbol{\Psi}_R$:

$$\left|\hat{z} - z_r\right| \leq \kappa_2'' \left\|\boldsymbol{U}_{r,1}\boldsymbol{\Psi}_r - \boldsymbol{U}_{r,2}\right\|_2 \tag{45}$$

where

$$\kappa_2'' = \frac{\sigma_{\max}\left(\begin{bmatrix} \boldsymbol{A}_1 \operatorname{diag}\{\boldsymbol{s}\} \\ \boldsymbol{A}_1 \operatorname{diag}\{\tilde{\boldsymbol{s}}\} \end{bmatrix}\right)}{\sigma_{\min}\left(\boldsymbol{A}_1 \operatorname{diag}\{\boldsymbol{s}\}\right)}. \tag{46}$$

Therefore, the signal number can be determined as

$$\hat{R}_{\mathrm{MDF-ESTER}} = \underset{r=1,2,\ldots,R_{\max}}{\arg\min} \left\|\boldsymbol{U}_{r,1}\boldsymbol{\Psi}_r - \boldsymbol{U}_{r,2}\right\|_2^2, \tag{47}$$

where $R_{\max}$ is stipulated by (40).

To maximize the number of detectable cisoids, $I_{1,n}$ and $I_{2,n}$, $n = 1, 2, \ldots, N$, are chosen as

$$\begin{cases} \text{if } I_n \text{ is even} & I_{1,n} = \frac{I_n}{2},\ I_{2,n} = \frac{I_n+2}{2} \\ \text{if } I_n \text{ is old} & I_{1,n} = I_{2,n} = \frac{I_n+1}{2}. \end{cases} \tag{48}$$

As a consequence, the maximum number of detectable cisoids is

$$R_{\max} = \prod_{n=1}^{N} \left\lceil \frac{I_n}{2} \right\rceil - 1 \tag{49}$$

For small sensor arrays or large dimensions N and when I_1 is odd, (49) represents a non-trivial gain in detectability over (32).

4. *N*-D sinusoidal order estimation using multidimensional folding: multiple-snapshot case

For the multiple-snapshot case, the size of the nonexponential/temporal dimension is $T > 1$. When T is sufficiently large, e.g., $T \geq I_1 I_2 \cdots I_N$, one of the N spatial dimensions of the $(N+1)$-D tensor $\mathcal{X}$ is used to construct the length-2 dimension indexed by $i_{\mathrm{SI},1}$, while the remaining dimensions stay unchanged, in the same line as [13] (cf. Section VI.C in [13]):

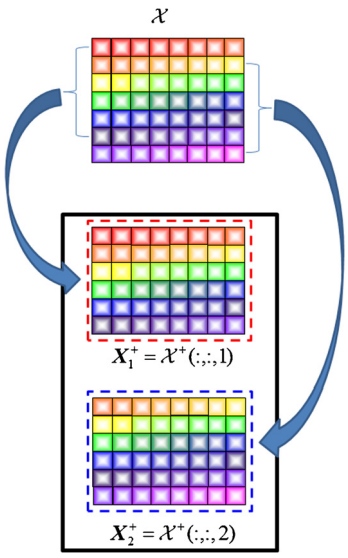

Fig. 5. Multiple-snapshot case: multidimensional folding/unfolding of a two-way array (i.e., matrix) $\mathcal{X}$ of size 7×8. Top: $\mathcal{X}$; Bottom: the two matrix slices of the three-way array $\mathcal{X}^+$ of size $6 \times 8 \times 2$ constructed via multidimensional folding and unfolding.

$$x^+_{i_{1,1},i_2,\ldots,i_N,t,i_{\mathrm{SI},1}} = x_{i_{1,1}+i_{\mathrm{SI},1}-1,i_2,\ldots,i_N,t},$$

where $i_{1,1} = 1, \ldots, I_{1,1} = I_1 - 1$, $i_{\mathrm{SI},1} = 1, 2$, and for ease of exposition of the algorithm, we have assumed that the first dimension is chosen for folding.

In the absence of noise, the resultant $(N+2)$-D tensor $\mathcal{X}^+ \in \mathbb{C}^{I_{1,1}\times I_2 \times \cdots \times I_N \times 2}$ can be represented in scalar form as

$$x^+_{i_{1,1},i_2,\ldots,i_N,t,i_{\mathrm{SI},1}} = \sum_{r=1}^{R} s_r(t) z_{r,1}^{i_{\mathrm{SI},1}-1} z_{r,1}^{i_{1,1}-1} \prod_{n=2}^{N} z_{r,n}^{i_n-1}, \tag{50}$$

and in tensor form as

$$\mathcal{X}^+ = \mathcal{I}_{N+2,R} \times_1 \boldsymbol{A}_1^{(1)} \times_2 \boldsymbol{A}^{(2)} \cdots \times_N \boldsymbol{A}^{(N)} \times_{N+1} \boldsymbol{S} \times_{N+2} \boldsymbol{A}_2^{(1)}, \tag{51}$$

where

$$\boldsymbol{A}_1^{(1)} = \begin{bmatrix} 1 & 1 & \cdots & 1 \\ z_{1,1} & z_{2,1} & \cdots & z_{R,1} \\ \vdots & \ddots & \vdots & \\ z_{1,1}^{I_{1,1}-1} & z_{2,1}^{I_{1,1}-1} & \cdots & z_{R,1}^{I_{1,1}-1} \end{bmatrix} \in \mathbb{C}^{I_{1,1}\times R}, \tag{52}$$

$$\boldsymbol{A}_2^{(1)} = \begin{bmatrix} 1 & 1 & \cdots & 1 \\ z_{1,1} & z_{2,1} & \cdots & z_{R,1} \end{bmatrix} \in \mathbb{C}^{2\times R}. \tag{53}$$

Denote the two matrix slices of $\mathcal{X}^+$ along the $(N+2)$-th dimension respectively as

$$\boldsymbol{X}_1^+ = \boldsymbol{A}\boldsymbol{S}^{\mathrm{T}} \in \mathbb{C}^{I_{1,1}I_2\ldots I_N\times T} \tag{54}$$

$$\boldsymbol{X}_2^+ = \boldsymbol{A}\boldsymbol{\Phi}^{(1)}\boldsymbol{S}^{\mathrm{T}} \in \mathbb{C}^{I_{1,1}I_2\ldots I_N\times T} \tag{55}$$

where

$$\boldsymbol{A} = \boldsymbol{A}^{(N)} \diamond \cdots \diamond \boldsymbol{A}^{(2)} \diamond \boldsymbol{A}_1^{(1)} \in \mathbb{C}^{I_{1,1}I_2\ldots I_N\times R}, \tag{56}$$

$$\boldsymbol{\Phi}^{(1)} = \operatorname{diag}\left\{\begin{bmatrix} z_{1,1} & z_{2,1} & \ldots & z_{R,1} \end{bmatrix}\right\}. \tag{57}$$

Fig. 5 illustrates the folding/unfolding process for a two-way tensor (i.e., matrix) of size 7×8, where $T = 8$ is the number of temporal snapshots.

According to Proposition 4 of [13], as the Khatri–Rao product of N Vandermonde matrices, $\boldsymbol{A}$ has full rank a.s. It follows that when

$$R \le \min(I_{1,1} I_2 \dots I_N, T), \tag{58}$$

we have

$$\boldsymbol{X}^+ = \begin{bmatrix} \boldsymbol{X}_1^+ \\ \boldsymbol{X}_2^+ \end{bmatrix} = \begin{bmatrix} \boldsymbol{A} \\ \boldsymbol{A}\boldsymbol{\Phi}^{(1)} \end{bmatrix} \boldsymbol{S}^{\mathrm{T}} \tag{59}$$

has rank R. Let

$$\boldsymbol{U}_r = \begin{bmatrix} \boldsymbol{U}_{r,1} \\ \boldsymbol{U}_{r,2} \end{bmatrix}, \tag{60}$$

with $\boldsymbol{U}_{r,b} \in \mathbb{C}^{I_{1,1} I_2 \dots I_N \times R}$, $b = 1, 2$, collect the r left singular vectors associated with the largest singular values of most columns of $\boldsymbol{X}^+$. In the absence of noise,

$$\boldsymbol{U}_R = \begin{bmatrix} \boldsymbol{U}_{R,1} \\ \boldsymbol{U}_{R,2} \end{bmatrix} \quad \text{and} \quad \begin{bmatrix} \boldsymbol{A} \\ \boldsymbol{A}\boldsymbol{\Phi}^{(1)} \end{bmatrix} \tag{61}$$

span the same subspace and hence there exists a non-singular matrix $\boldsymbol{T} \in \mathbb{C}^{R \times R}$ such that

$$\begin{bmatrix} \boldsymbol{A} \\ \boldsymbol{A}\boldsymbol{\Phi}^{(1)} \end{bmatrix} = \begin{bmatrix} \boldsymbol{U}_{R,1} \\ \boldsymbol{U}_{R,2} \end{bmatrix} \boldsymbol{T}. \tag{62}$$

It then follows that

$$\boldsymbol{U}_{R,1} \boldsymbol{\Psi}_R = \boldsymbol{U}_{R,2} \tag{63}$$

where $\boldsymbol{\Psi}_R = \boldsymbol{T}\boldsymbol{\Phi}^{(1)}\boldsymbol{T}^{-1}$.

4.1. Order selection based on estimation error

Define

$$\boldsymbol{\Psi}_r = \boldsymbol{U}_{r,1}^{\dagger} \boldsymbol{U}_{r,2}. \tag{64}$$

In the case of $r < R$, in a similar way of [26] and Theorem 3.1, we can prove that in the absence of noise, $\left\| \boldsymbol{U}_{r,1}\boldsymbol{\Psi}_r - \boldsymbol{U}_{r,2} \right\|_2$ is lower bounded by the absolute difference between an eigenvalue $\hat{z}$ of $\boldsymbol{\Psi}_r$ and its closest eigenvalue $z_r \in \{z_{1,1}, z_{2,1}, \dots, z_{R,1}\}$ of $\boldsymbol{\Psi}_R$:

$$\left| \hat{z} - z_r \right| \le \kappa_2' \left\| \boldsymbol{U}_{r,1}\boldsymbol{\Psi}_r - \boldsymbol{U}_{r,2} \right\|_2 \tag{65}$$

where

$$\kappa_2' = \frac{\sigma_{\max}\left(\begin{bmatrix} \boldsymbol{A} \\ \boldsymbol{A}\boldsymbol{\Phi}^{(1)} \end{bmatrix} \right)}{\sigma_{\min}(\boldsymbol{A})}. \tag{66}$$

When $r > R$, it also holds that $\|\boldsymbol{E}_r\|_2 > 0$ following a similar argument of Section 3.1 (see the note therein). Therefore, in the absence of noise the minimum of zero of $\|\boldsymbol{E}_r\|_2$ is reached only at $r = R$. When noise is present, the signal number can be estimated by minimizing the estimation error:

$$\hat{R}_{\mathrm{MDF-ESTER}} = \underset{r=1,2,\dots,R_{\max}}{\arg\min} \left\| \boldsymbol{U}_{r,1}\boldsymbol{\Psi}_r - \boldsymbol{U}_{r,2} \right\|_2^2. \tag{67}$$

Taking into account that $I_{1,1} = I_1 - 1$, it follows that the maximum number of detectable signals is

$$\begin{aligned} R_{\max} &= \min(I_{1,1} I_2 \cdots I_N - 1, T) \\ &= \min\left(I_1 I_2 \cdots I_N \left[1 - \frac{1}{I_1} \right] - 1, T \right). \end{aligned} \tag{68}$$

By choosing the dimension of maximum length $n_0 = \arg\max_n I_n$ for folding, the maximum number of detectable signals is increased to

$$R_{\max} = \min\left(I_1 I_2 \cdots I_N \left[1 - \frac{1}{I_{n_0}} \right] - 1, T \right). \tag{69}$$

4.2. Small temporal sample-size scenario

When T is relatively small, e.g., $T \ll I_1 I_2 \cdots I_N$, the identifiability stipulated by (69) is limited. To handle that, one or more spatial dimensions can be transformed/splitted into two dimensions via MDF. For instance, suppose $n_0 = 1$ in (69) and folding the second spatial dimension yields

$$\begin{aligned} & x^+_{i_{1,1}, i_{1,2}, i_{2,2}, i_3, \dots, i_N, t, i_{\mathrm{SI},1}} \\ &\quad = x_{i_{1,1} + i_{\mathrm{SI},1} - 1, i_{1,2} + i_{2,2} - 1, i_3, \dots, i_N, t}, \\ &\quad = \sum_{r=1}^{R} z_{r,1}^{i_{1,1}-1} z_{r,2}^{i_{1,2}-1} z_{r,2}^{i_{2,2}-1} \prod_{n=3}^{N} z_{r,n}^{i_n - 1} \cdot s_r(t) \cdot z_{r,1}^{i_{\mathrm{SI},1}-1}, \end{aligned} \tag{70}$$

where $i_{1,1} = 1, \dots, I_1 - 1$, $i_{\mathrm{SI},1} = 1, 2$, $i_{1,2} = 1, 2, \dots, I_{1,2}$, $i_{2,2} = 1, 2, \dots, I_{2,2}$, with $I_{1,2} + I_{2,2} = I_2 + 1$.

In tensor form, (70) is expressed as

$$\begin{aligned} \mathcal{X}^+ = \mathcal{I}_{N+3,R} \times_1 \boldsymbol{A}_1^{(1)} \times_2 \boldsymbol{A}_1^{(2)} \times_3 \boldsymbol{A}_2^{(2)} \times_4 \boldsymbol{A}^{(3)} \dots \\ \times_{N+1} \boldsymbol{A}^{(N)} \times_{N+2} \boldsymbol{S} \times_{N+3} \boldsymbol{A}_2^{(1)}, \end{aligned} \tag{71}$$

where $\boldsymbol{A}_b^{(1)}$ and $\boldsymbol{A}_b^{(2)}$, $b = 1, 2$, are defined in (52)–(53) and (8)–(9), respectively.

By merging/unfolding/collapsing the $1, 2, 4, \dots, N+1$ dimensions and $3, N+2$ dimensions of $\mathcal{X}^+$ into one dimension, respectively, we obtain

$$\overline{\mathcal{X}^+} = \mathcal{I}_{3,R} \times_1 \tilde{\boldsymbol{A}} \times_2 \tilde{\boldsymbol{S}} \times_3 \boldsymbol{A}_2^{(1)}, \tag{72}$$

where

$$\tilde{\boldsymbol{A}} = \boldsymbol{A}^{(N)} \diamond \cdots \diamond \boldsymbol{A}^{(3)} \diamond \boldsymbol{A}_1^{(2)} \diamond \boldsymbol{A}_1^{(1)} \in \mathbb{C}^{I_{1,1} I_{1,2} I_3 \cdots I_N \times R}, \tag{73}$$

$$\tilde{\boldsymbol{S}} = \boldsymbol{A}_2^{(2)} \diamond \boldsymbol{S} \in \mathbb{C}^{I_{2,2} T \times R}. \tag{74}$$

The two matrix slices of $\mathcal{X}^+$ along the third dimension are

$$\boldsymbol{X}_1^+ = \tilde{\boldsymbol{A}} \tilde{\boldsymbol{S}}^{\mathrm{T}} \in \mathbb{C}^{I_{1,1} I_{1,2} I_3 \cdots I_N \times I_{2,2} T} \tag{75}$$

$$\boldsymbol{X}_2^+ = \tilde{\boldsymbol{A}} \boldsymbol{\Phi}^{(1)} \tilde{\boldsymbol{S}}^{\mathrm{T}} \in \mathbb{C}^{I_{1,1} I_{1,2} I_3 \cdots I_N \times I_{2,2} T} \tag{76}$$

where

$$\boldsymbol{\Phi}^{(1)} = \mathrm{diag}\left\{ \begin{bmatrix} z_{1,1} & z_{2,1} & \dots & z_{R,1} \end{bmatrix} \right\}. \tag{77}$$

Following similar arguments as previous sections, the maximum number of detectable signals is increased to

$$R_{\max} = \min(I_{1,1} I_{1,2} I_3 \cdots I_N - 1, I_{2,2} T). \tag{78}$$

When the temporal sample-size is small, e.g., $T \ll I_1 I_2 \cdots I_N$, (78) represents a non-trivial gain in detectability over (68).

5. Simulation results

We present simulation results demonstrating the performance of the proposed MDF-ESTER schemes in Sections 3 and 4. The measurement data are generated based on the N-D undamped HR model, namely, (1) with $\zeta_f^{(n)} = 0$, where the spatial frequencies $\mu_r^{(n)}$ are drawn from a uniform distribution in $[-\pi, \pi]$. The signal symbols are uncorrelated zero-mean circularly symmetric complex Gaussian (ZMCSCG) random variables with identical power of σ_s^2.

Along the same line as [33,44], the multidimensional colored noise is assumed to have a Kronecker structure:

$$\mathcal{N}^{(\mathrm{C})} = \mathcal{N} \times_1 \boldsymbol{L}_1 \times_2 \boldsymbol{L}_2 \cdots \times_N \boldsymbol{L}_N. \tag{79}$$

where $\mathcal{N} \in \mathbb{C}^{I_1 \times \cdots \times I_N \times T}$ is a tensor collecting the i.i.d. ZMCSCG noise samples with variance σ_n^2, and $\boldsymbol{L}_n \in \mathbb{C}^{I_n \times I_n}$, $n = 1, 2, \dots, N$,

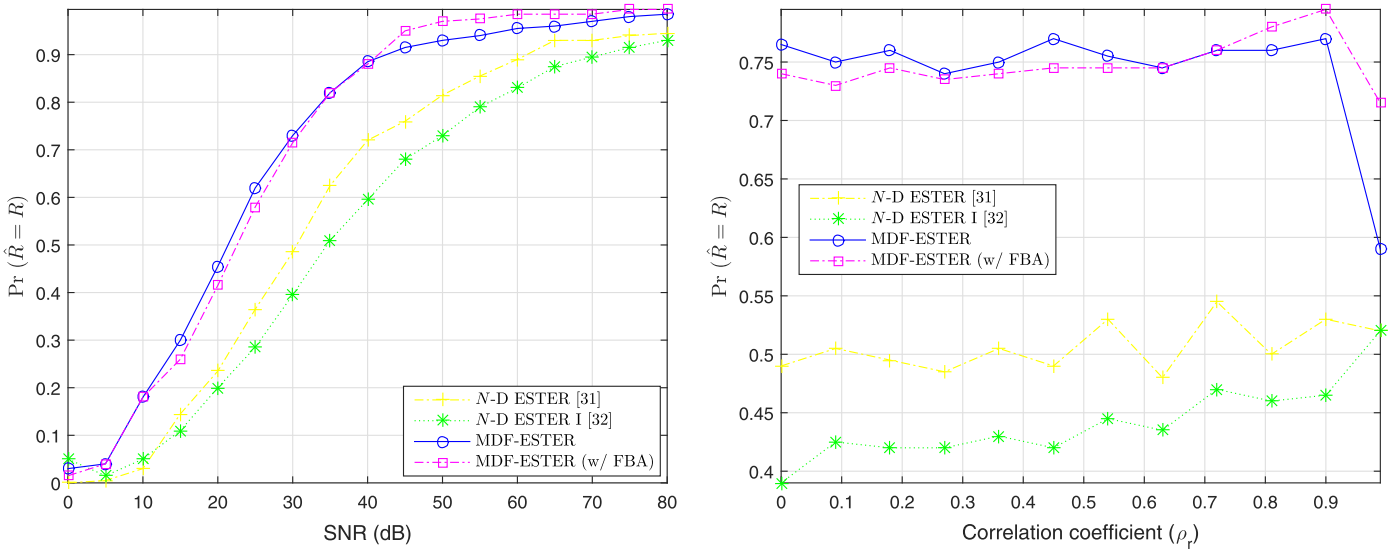

(a) PoD versus SNR. ρ_n = 0.125

(b) PoD versus ρ_n. SNR=30 dB

Fig. 6. Probability of correct detection for single-snapshot HR ($T = 1$) in Kronecker colored noise environment. In the simulated scenario, $N = 2$, $I_1 = I_2 = 7$, and the number of signals is $R = 4$.

is the correlation factor in the n-th dimension of the colored noise tensor. The signal-to-noise ratio (SNR) is defined as

$$\text{SNR} = \frac{\|\mathcal{X}\|_{\text{F}}^2}{\sigma_n^2 \prod_{n=1}^{N} I_n}.$$

The noise power σ_n^2 is scaled to obtain different SNRs. For each SNR, 200 independent Monte Carlo runs have been conducted.

As in [33,44], the colored noise is modeled as a first-order autoregressive process:

$$n_{m+1}^{(\text{c})} = \rho_n \cdot n_m^{(\text{c})} + \sqrt{1 - \rho_n^2} \cdot n_{m+1}, \tag{80}$$

such that the noise covariance matrix $\boldsymbol{C}_n = \boldsymbol{L}_n \boldsymbol{L}_n^{\text{H}}$, $n = 1, 2, \ldots, N$, is a function of a single variable, namely, the correlation coefficient ρ_n. As an example, $\boldsymbol{C}_n$ for $I_n = 3$ has the following structure

$$\boldsymbol{C}_n = \begin{bmatrix} 1 & \rho_n^* & (\rho_n^*)^2 \\ \rho_n & 1 & \rho_n^* \\ \rho_n^2 & \rho_n & 1 \end{bmatrix}. \tag{81}$$

Note that similar simulation results are observed for other types of noise correlation models.

The performance measure is the PoD, i.e., $\Pr(\hat{R} = R)$. The PoD's of the following schemes are used as the benchmark: the original N-D ESTER proposed in [32] and its two variants proposed in [33]. The MATLAB codes of all order selection algorithms can be downloaded at http://www.ee.cityu.edu.hk/~hcso/publication.html.

5.1. Single-snapshot HR model

For a single-snapshot ($T = 1$) HR model we evaluate the MDF-ESTER proposed in Section 3. Note that for single-snapshot HR model, the N-D ESTER II [33] is not applicable since $T < R$.[4]

We consider a 2-D array with $I_1 = I_2 = 7$. In Fig. 6(a), the PoDs versus SNR of different order selection schemes are compared for $R = 4$ signals, where the correlation coefficients of the colored noise are set as $\rho_1 = \rho_2 = \rho_3 = 0.125$. We see that the MDF-ESTER outperforms the original N-D ESTER [32] and N-D ESTER I [33]. The MDF-ESTER with FBA performs the best. In Fig. 6(b), the order selection schemes are evaluated for various noise correlation levels, where the SNR is fixed at 30 dB. Here, the correlation coefficients are equal to each other and vary from 0 to 0.999. Note that the MDF-ESTER keeps almost a constant PoD regardless of the noise correlation levels except for very high noise correlation levels.

In Fig. 7, the number of signals is increased from 4 to 8. The N-D ESTERs totally fail since they can detect at most 5 signals, as shown in Table 1. Similar observations are obtained except for a larger performance gap between the MDF-ESTER without and with FBA.

5.2. Multiple-snapshot HR model

For a multiple-snapshot ($T > 1$) HR model we evaluate the MDF-ESTER proposed in Section 4.

In Fig. 8, we have the same scenario as in Figs. 6 and 7, the number of snapshots is increased from $T = 1$ to $T = 125$. We observe a performance improvement of all algorithms compared to Fig. 6. In addition, Fig. 8(b) indicates a weaker robustness of all algorithms compared to Figs. 6(b) and 7(b). With the increase of the noise correlation level, the PoDs of all algorithms show a slight (but clear) decrease for low-to-intermediate ρ_n followed by a sharp drop for high $\rho_n > 0.8$.

Moreover, for such a multiple-snapshot scenario with sufficiently large T, the MDF-ESTER can detect much more signals compared to the single-snapshot case. Fig. 9 shows that at $R = 32$ the MDF-ESTER is still able to detect the number of signals with a probability of one for sufficiently high SNRs.

The maximum numbers of detectable signals of the N-D ESTER methods and our proposed MDF-ESTER for the single-snapshot and multiple-snapshot scenarios are summarized in Table 1.

[4] The N-D ESTER II relies on the tensor shift invariance equation (defined in (20) of [33]) and that in the absence of noise the tensor signal subspace represented by $\mathcal{U}$ (defined in (21) of [33]) and the array steering tensor $\mathcal{A}$ (defined in (7) of [33]) span the same subspace in all n-modes. The tensor signal subspace $\mathcal{U}$ is estimated by performing truncation in the HOSVD. In case of $T < R$, the problem is degenerate in the temporal mode. As a result, the estimated $\mathcal{U}$ via the HOSVD will be of rank at most T and less than R, and $\mathcal{U}$ cannot span the same subspace as $\mathcal{A}$ in the absence of noise.

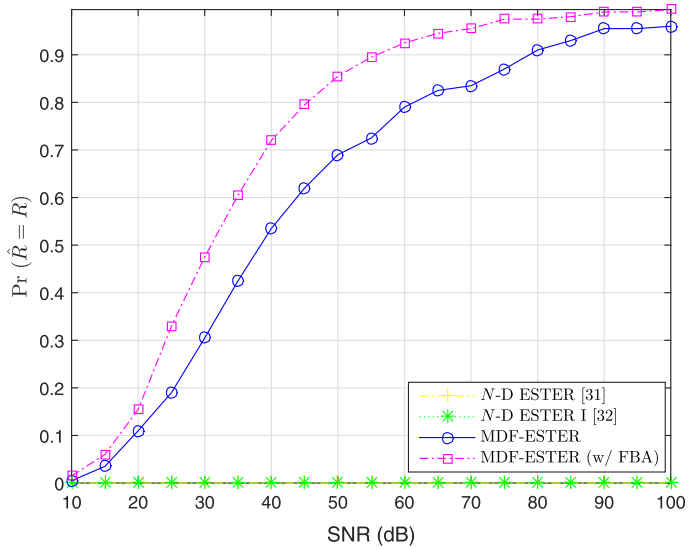

(a) PoD versus SNR. ρ_n = 0.125

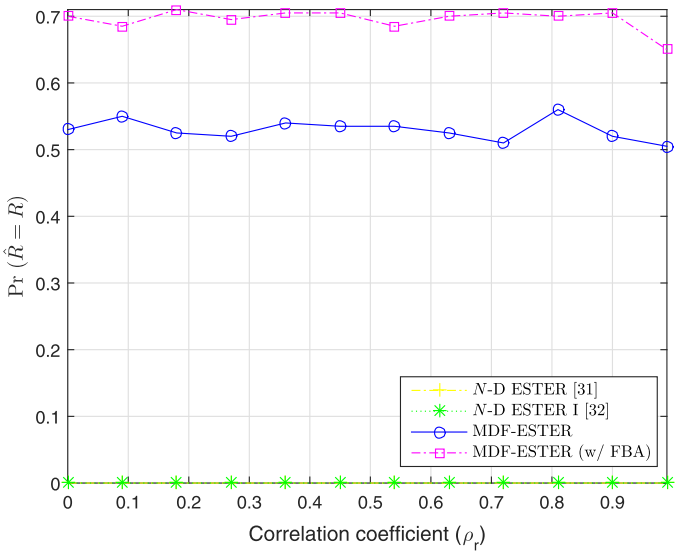

(b) PoD versus ρ_n. SNR=40 dB

Fig. 7. Probability of correct detection for single-snapshot HR ($T = 1$) in Kronecker colored noise environment. In the simulated scenario, $N = 2$, $I_1 = I_2 = 7$, and the number of signals is $R = 8$.

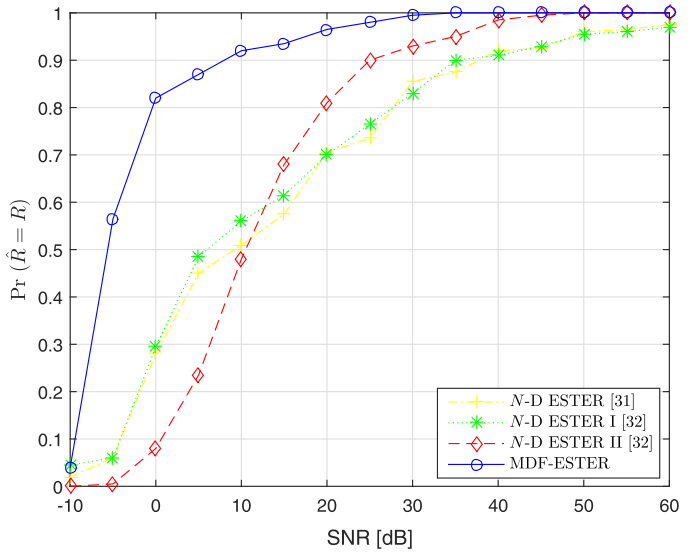

(a) PoD versus SNR. ρ_n = 0.125

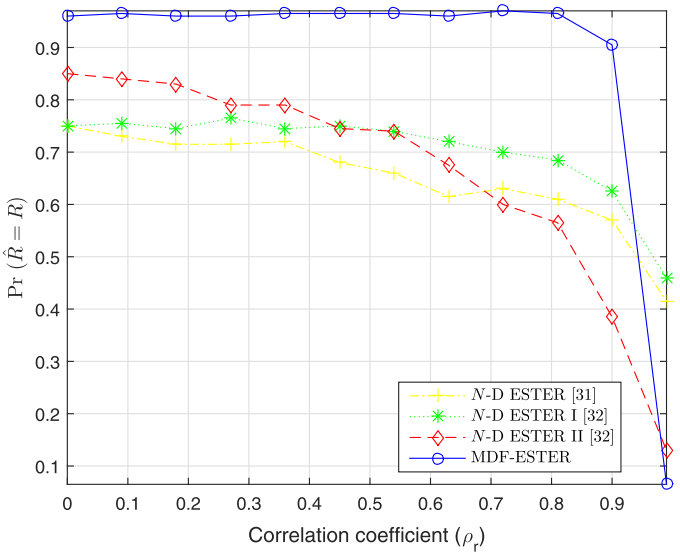

(b) PoD versus ρ_n. SNR=20 dB

Fig. 8. Probability of correct detection for multiple-snapshot HR in Kronecker colored noise environment. In the simulated scenario, $N = 2$, $I_1 = I_2 = 7$, the number of temporal snapshots is $T = 125$, and the number of signals is $R = 4$.

Table 1
Comparison of the N-D ESTER methods and our proposed MDF-ESTER in terms of maximum number of detectable signals for the simulated single-snapshot ($T = 1$) and multiple-snapshot ($T = 125$) scenarios. $I_1 = I_2 = 7$.

	Original R-D ESTER [32]	R-D ESTER I [33]	R-D ESTER II [33]	MDF-ESTER	MDF-ESTER (w/ FBA)
$T = 1$	5	5	–	11	15
$T = 125$	5	5	5	41	–

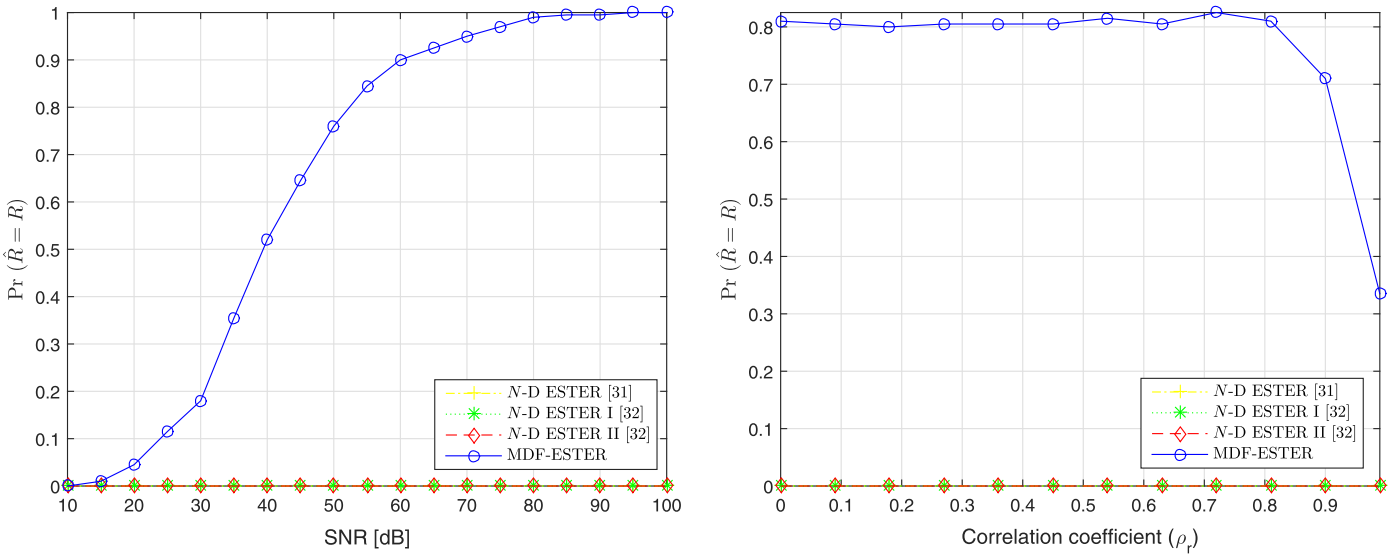

(a) PoD versus SNR. $\rho_n = 0.125$

(b) PoD versus ρ_n. SNR=50 dB

Fig. 9. Probability of correct detection for multiple-snapshot HR in Kronecker colored noise environment. In the simulated scenario, $N = 2$, $I_1 = I_2 = 7$, the number of temporal snapshots is $T = 125$, and the number of signals is $R = 32$.

6. Conclusion

Multidimensional sinusoidal order selection is required in many applications. The ESTER is a subspace based detection approach that is robust against colored noise. We propose to combine the MDF techniques with the ESTER for multidimensional sinusoidal order selection. Based on the observation that the two matrix slices resulting from multidimensional folding and embedding satisfy the shift invariance equation, the ESTER criterion is employed to estimate the sinusoidal order. Compared to state-of-the-art multidimensional ESTERs, the MDF-ESTER can detect significantly much more signals. Meanwhile, it retains the advantage of the ESTER in terms of robustness against colored noise, and is thus suitable for colored noise environments. As a future work, we will evaluate the proposed algorithms on real-world data sets.

Appendix A. Proof of Theorem 3.1

Proof. If $\hat{z} = z_r$ for some $r \in \{1, \ldots, R\}$, the inequality (27) trivially holds, since the left-hand side is equal to zero. So we may assume that $\hat{z} \neq z_r$ for all $r \in \{1, \ldots, R\}$.

Let $\boldsymbol{v} \in \mathbb{C}^{r\times 1}$ be the eigenvector associated with $\hat{z}$, i.e., $\boldsymbol{\Psi}_r \boldsymbol{v} = \hat{z}\boldsymbol{v}$, and define

$$\boldsymbol{e}(r) = \left(\boldsymbol{U}_{r,2} - \boldsymbol{U}_{r,1}\boldsymbol{\Psi}_r\right)\boldsymbol{v} = \left(\boldsymbol{U}_{r,2} - \hat{z}\boldsymbol{U}_{r,1}\right)\boldsymbol{v}. \tag{A.1}$$

Note that

$$\boldsymbol{U}_{r,1}\boldsymbol{v} = \boldsymbol{U}_{R,1}\begin{bmatrix}\boldsymbol{v}\\ \boldsymbol{0}_{R-r}\end{bmatrix}, \quad \boldsymbol{U}_{r,2}\boldsymbol{v} = \boldsymbol{U}_{R,2}\begin{bmatrix}\boldsymbol{v}\\ \boldsymbol{0}_{R-r}\end{bmatrix},$$

so that

$$\boldsymbol{e}(r) = \left(\boldsymbol{U}_{R,2} - \hat{z}\boldsymbol{U}_{R,1}\right)\begin{bmatrix}\boldsymbol{v}\\ \boldsymbol{0}_{R-r}\end{bmatrix}. \tag{A.2}$$

From (24) it follows that $\boldsymbol{U}_{R,1} = \boldsymbol{A}_1\boldsymbol{T}^{-1}$ and $\boldsymbol{U}_{R,2} = \boldsymbol{A}_1\boldsymbol{\Phi}^{(1)}\boldsymbol{T}^{-1}$. Then (A.2) becomes

$$\boldsymbol{e}(r) = \boldsymbol{A}_1\left(\boldsymbol{\Phi}^{(1)} - \hat{z}\boldsymbol{I}_R\right)\boldsymbol{T}^{-1}\begin{bmatrix}\boldsymbol{v}\\ \boldsymbol{0}_{R-r}\end{bmatrix}. \tag{A.3}$$

Since $\hat{z} \neq z_r$ for all $r \in \{1, \ldots, R\}$, $\boldsymbol{\Phi}^{(1)} - \hat{z}\boldsymbol{I}_R$ is non-singular. Therefore,

$$\begin{bmatrix}\boldsymbol{v}\\ \boldsymbol{0}_{R-r}\end{bmatrix} = \boldsymbol{T}\left(\boldsymbol{\Phi}^{(1)} - \hat{z}\boldsymbol{I}_R\right)^{-1}\boldsymbol{A}_1^{\dagger}\boldsymbol{e}(r). \tag{A.4}$$

Taking the spectral norm on both sides of (A.4), we obtain

$$\|\boldsymbol{v}\|_2 \leq \|\boldsymbol{T}\|_2 \left\|\left(\boldsymbol{\Phi}^{(1)} - \hat{z}\boldsymbol{I}_R\right)^{-1}\right\|_2 \left\|\boldsymbol{A}_1^{\dagger}\right\|_2 \|\boldsymbol{e}(r)\|_2. \tag{A.5}$$

Since

$$\begin{bmatrix}\boldsymbol{A}_1\\ \boldsymbol{A}_1\boldsymbol{\Phi}^{(1)}\end{bmatrix} = \boldsymbol{U}_R\boldsymbol{T} \tag{A.6}$$

and $\boldsymbol{U}_R$ has orthonormal columns, it holds that

$$\|\boldsymbol{T}\|_2 = \left\|\begin{bmatrix}\boldsymbol{A}_1\\ \boldsymbol{A}_1\boldsymbol{\Phi}^{(1)}\end{bmatrix}\right\|_2 = \sigma_{\max}\left(\begin{bmatrix}\boldsymbol{A}_1\\ \boldsymbol{A}_1\boldsymbol{\Phi}^{(1)}\end{bmatrix}\right).$$

Moreover, $\left(\boldsymbol{\Phi}^{(1)} - \hat{z}\boldsymbol{I}_R\right)^{-1}$ is a diagonal matrix with diagonal entries $1/(z_r - \hat{z})$, thus

$$\left\|\left(\boldsymbol{\Phi}^{(1)} - \hat{z}\boldsymbol{I}_R\right)^{-1}\right\|_2 = \frac{1}{\min\limits_{r\in\{1,\ldots,R\}}\left|\hat{z} - z_r\right|}.$$

Also considering that $\left\|\boldsymbol{A}_1^{\dagger}\right\|_2 = \frac{1}{\sigma_{\min}(\boldsymbol{A}_1)}$, and $\boldsymbol{v}$ is unitary, it follows from (A.5) that

$$\min_{r\in\{1,\ldots,R\}}\left|\hat{z} - z_r\right| \leq \frac{\sigma_{\max}\left(\begin{bmatrix}\boldsymbol{A}_1\\ \boldsymbol{A}_1\boldsymbol{\Phi}^{(1)}\end{bmatrix}\right)}{\sigma_{\min}(\boldsymbol{A}_1)}\|\boldsymbol{e}(r)\|_2. \tag{A.7}$$

From (A.1), we have

$$\|\boldsymbol{e}(r)\|_2 \leq \left\|\boldsymbol{U}_{r,2} - \hat{z}\boldsymbol{U}_{r,1}\right\|_2. \tag{A.8}$$

The conclusion (27) follows by combining (A.7) with (A.8). □

Appendix B. Supplementary material

Supplementary material related to this article can be found online at http://dx.doi.org/10.1016/j.dsp.2015.10.001.

References

[1] M. Pesavento, Fast algorithm for multidimensional harmonic retrieval, Ph.D. thesis, Electrical Engineering and Information Sciences, Ruhr-Universität Bochum, Bochum, Germany, Feb. 2005.

[2] D. Nion, N.D. Sidiropoulos, Tensor algebra and multidimensional harmonic retrieval in signal processing for MIMO radar, IEEE Trans. Signal Process. 58 (11) (2010) 5693–5705.

[3] M. Haardt, C. Brunner, J.H. Nossek, Efficient high-resolution 3-D channel sounding, in: Proc. 48th IEEE Vehicular Technology Conference, VTC, Ottawa, ON, Canada, 1998, pp. 164–168.

[4] K.N. Mokios, N.D. Sidiropoulos, M. Pesavento, C.E. Mecklenbrauker, On 3-D harmonic retrieval for wireless channel sounding, in: Proc. International Conference on Acoustics, Speech, and Signal Processing, vol. 2, ICASSP, 2004, pp. 89–92.

[5] M. Haardt, R.S. Thomä, A. Richter, Multidimensional high-resolution parameter estimation with applications to channel sounding, in: Y. Hua, A. Gershman, Q. Chen (Eds.), High-Resolution and Robust Signal Processing, Marcel Dekker, New York, NY, 2004, pp. 255–338, chapter 5.

[6] A. Bax, L. Lerner, Two-dimensional NMR spectroscopy, Science 232 (4753) (1986) 960–967.

[7] Y. Li, J. Razavilar, K. Liu, A high-resolution technique for multidimensional NMR spectroscopy, IEEE Trans. Biomed. Eng. 45 (1998) 78–86.

[8] M.D. Zoltowski, M. Haardt, C.P. Mathews, Closed-form 2D angle estimation with rectangular arrays in element space or beamspace via unitary ESPRIT, IEEE Trans. Signal Process. 44 (2) (1996) 316–328.

[9] M. Haardt, J.A. Nossek, Simultaneous Schur decomposition of several nonsymmetric matrices to achieve automatic pairing in multidimensional harmonic retrieval problems, IEEE Trans. Signal Process. 46 (1) (1998) 161–169.

[10] M. Haardt, F. Römer, G. Del Galdo, Higher-order SVD based subspace estimation to improve the parameter estimation accuracy in multi-dimensional harmonic retrieval problems, IEEE Trans. Signal Process. 56 (7) (2008) 3198–3213.

[11] A. Thakre, M. Haardt, K. Giridhar, Single snapshot R-D unitary tensor-ESPRIT using an augmentation of the tensor order, in: Proc. IEEE International Workshop on Computational Advances in Multi-Sensor Adaptive Processing, Aruba, Dutch Antilles, 2009, pp. 81–84.

[12] H.L. Van Trees, Optimum Array Processing: Detection, Estimation, and Modulation Theory, Wiley, New York, 2002, Part IV.

[13] T. Jiang, N.D. Sidiropoulos, J.M.F. ten Berge, Almost-sure identifiability of multidimensional harmonic retrieval, IEEE Trans. Signal Process. 49 (9) (2001) 1849–1859.

[14] X. Liu, N.D. Sidiropoulos, Almost sure identifiability of constant modulus multidimensional harmonic retrieval, IEEE Trans. Signal Process. 50 (9) (2002) 2366–2368.

[15] J. Liu, X. Liu, An eigenvector-based approach for multidimensional frequency estimation with improved identifiability, IEEE Trans. Signal Process. 54 (12) (2006) 4543–4556.

[16] M. Pesavento, C.F. Mecklenbräuker, J.F. Böhme, Multidimensional rank reduction estimator for parametric MIMO channel models, EURASIP J. Appl. Signal Process. (2004) 1354–1363.

[17] F.K.W. Chan, H.C. So, W. Sun, Subspace approach for two-dimensional parameter estimation of multiple damped sinusoids, Signal Process. 92 (9) (2012) 2172–2179.

[18] W. Sun, H.C. So, Accurate and computationally efficient tensor-based subspace approach for multi-dimensional harmonic retrieval, IEEE Trans. Signal Process. 60 (10) (2012) 5077–5088.

[19] P. Stoica, Y. Selen, Model-order selection: a review of information criterion rules, IEEE Signal Process. Mag. 21 (4) (2004) 36–47.

[20] M. Wax, T. Kailath, Detection of signals by information theoretic criteria, IEEE Trans. Acoust. Speech Signal Process. 33 (2) (1985) 387–392.

[21] H. Akaike, A new look at the statistical model identification, IEEE Trans. Autom. Control 19 (6) (1974) 716–723.

[22] S. Kritchman, B. Nadler, Determining the number of components in a factor model from limited noisy data, Chemom. Intell. Lab. Syst. 94 (2008) 19–32.

[23] S. Kritchman, B. Nadler, Non-parametric detection of the number of signals: hypothesis testing and random matrix theory, IEEE Trans. Signal Process. 57 (10) (2009) 3930–3941.

[24] R.R. Nadakuditi, A. Edelman, Sample eigenvalue based detection of high-dimensional signals in white noise using relatively few samples, IEEE Trans. Signal Process. 56 (7) (2008) 2625–2638.

[25] L. Huang, C. Qian, H.C. So, J. Fang, Source enumeration for large array using shrinkage-based detectors with small samples, IEEE Trans. Aerosp. Electron. Syst. 51 (1) (Jan. 2015) 334–357.

[26] R. Badeau, B. David, G. Richard, Selecting the modeling order for the ESPRIT high resolution method: an alternative approach, in: Proc. IEEE International Conference on Acoustics, Speech and Signal Processing, vol. 2, ICASSP, Montreal, Canada, 2004, pp. 1025–1028.

[27] J.-M. Papy, L. de Lathauwer, S. van Huffel, A shift invariance-based order-selection technique for exponential data modeling, IEEE Signal Process. Lett. 14 (2007) 473–476.

[28] A. Di, Multiple source location—a matrix decomposition approach, IEEE Trans. Acoust. Speech Signal Process. 33 (5) (1985) 1086–1091.

[29] H.T. Wu, J.-F. Yang, F.-K. Chen, Source number estimators using transformed Gerschgorin radii, IEEE Trans. Signal Process. 43 (6) (1995) 1325–1333.

[30] L. Huang, T. Long, S. Wu, Source enumeration for high-resolution array processing using improved Gerschgorin radii without eigendecomposition, IEEE Trans. Signal Process. 56 (12) (2008) 5916–5925.

[31] R. Badeau, B. David, G. Richard, A new perturbation analysis for signal enumeration in rotational invariance techniques, IEEE Trans. Signal Process. 54 (2) (2006) 450–458.

[32] J.P.C.L. da Costa, F. Römer, D. Schulz, R. de Sousa, Subspace based multidimensional model order selection in colored noise scenarios, in: Proc. IEEE Information Theory Workshop, ITW, Paraty, Brazil, 2011, pp. 380–384.

[33] K. Liu, J.P.C.L. da Costa, H.C. So, L. Huang, Subspace techniques for multidimensional model order selection in colored noise, Signal Process. 93 (7) (2013) 1976–1987.

[34] D.A. Linebarger, R.D. DeGroat, E.M. Dowling, Efficient direction-finding methods employing forward/backward averaging, IEEE Trans. Signal Process. 42 (8) (1994) 2136–2145.

[35] L. de Lathauwer, B. de Moor, J. Vanderwalle, A multilinear singular value decomposition, SIAM J. Matrix Anal. Appl. 21 (4) (2000) 1253–1278.

[36] X.-D. Zhang, Y.-D. Li, Harmonic retrieval in mixed Gaussian and non-Gaussian ARMA noises, IEEE Trans. Signal Process. 42 (12) (1994) 3539–3543.

[37] X.-D. Zhang, Y.-C. Liang, Y.-D. Li, A hybrid approach to harmonic retrieval in non-Gaussian ARMA noise, IEEE Trans. Inf. Theory 40 (4) (1994) 1220–1226.

[38] B.M. Sadler, G.B. Giannakis, S. Shamsunder, Noise subspace techniques in non-Gaussian noise using cumulants, IEEE Trans. Aerosp. Electron. Syst. 31 (3) (1995) 1009–1018.

[39] Y. Zhang, S. Wang, Harmonic retrieval in colored non-Gaussian noise using cumulants, IEEE Trans. Signal Process. 48 (4) (2000) 982–987.

[40] T.G. Kolda, B.W. Bader, Tensor decompositions and applications, SIAM Rev. 51 (3) (2009) 455–500.

[41] S. Ragnarsson, C.F. Van Loan, Block tensor unfoldings, SIAM J. Matrix Anal. Appl. 33 (1) (2012) 149–169.

[42] K. Liu, H.C. So, L. Huang, A multi-dimensional model order selection criterion with improved identifiability, in: Proc. International Conference on Acoustics, Speech, and Signal Processing, ICASSP, Kyoto, Japan, 2012, pp. 2441–2444.

[43] R. Roy, T. Kailath, ESPRIT—estimation of signal parameters via rotational invariance techniques, IEEE Trans. Acoust. Speech Signal Process. ASSP-37 (1989) 984–995.

[44] J.P.C.L. da Costa, K. Liu, H.H.C. So, S. Schwarz, M. Haardt, F. Römer, Multidimensional prewhitening for enhanced signal reconstruction and parameter estimation in colored noise with Kronecker correlation structure, Signal Process. 93 (11) (2013) 3209–3226.

Kefei Liu is currently a Postdoctoral Research Fellow at the Department of Computational Medicine and Bioinformatics, University of Michigan. Before joining UMich, he received the B.Sc. degree in mathematics from Wuhan University in 2006 and Ph.D. degree in Electronic Engineering from City University of Hong Kong in 2013. In 2014, he was a Postdoctoral Research Fellow at the Center for Evolutionary Medicine and Informatics of The Biodesign Institute, Arizona State University. His research interests are tensor decompositions for machine learning and data mining, structured matrix/tensor completion, and bioinformatics.

Lei Huang (M'07–SM'14) was born in Guangdong, China. He received the B.Sc., M.Sc., and Ph.D. degrees in electronic engineering from Xidian University, Xidian, China, in 2000, 2003, and 2005, respectively.

From 2005 to 2006, he was a Research Associate with the Department of Electrical and Computer Engineering, Duke University, Durham, NC. From 2009 to 2010, he was a Research Fellow with the Department of Electronic Engineering, City University of Hong Kong and a Research Associate with the Department of Electronic Engineering, The Chinese University of Hong Kong. From 2011 to 2014, he was a Professor with the Department of Electronic and Information Engineering, Harbin Institute of Technology Shenzhen Graduate School. Since November 2014, he has joined the Department of Information Engineering, Shenzhen University, where he is currently a Chair Professor. His research interests include spectral estimation, array signal processing, statistical signal processing, and their applications in radar and wireless communication systems.

He is currently serving as an Associate Editor for IEEE Transactions on Signal Processing and Digital Signal Processing.

Hing Cheung So was born in Hong Kong. He received the B.Eng. degree from City University of Hong Kong (CityU) and the Ph.D. degree from The Chinese University of Hong Kong (CUHK), both in electronic engineering, in 1990 and 1995, respectively. From 1990 to 1991, he was an Electronic Engineer at the Research and Development Division, Everex Systems Engineering Ltd., Hong Kong. During 1995–1996, he worked as a Postdoctoral Fellow at CUHK. From 1996 to 1999, he was a Research Assistant Professor at Department of Electronic Engineering, CityU, where he is currently an Associate Professor. His research interests include detection and estimation, fast and adaptive algorithms, multidimensional harmonic retrieval, robust signal processing, source localization, and sparse approximation. He has been on the editorial boards of IEEE Signal Processing Magazine (2014–), IEEE Transactions on Signal Processing (2010–2014), Signal Processing (2010–), and Digital Signal Processing (2011–). In addition, he is an elected member in Signal Processing Theory and Methods Technical Committee (2011–) of the IEEE Signal Processing Society where he is chair in the awards subcommittee (2015). He has been elected Fellow of IEEE in recognition of his contributions to spectral analysis and source localization in 2015.

Jieping Ye received the Ph.D. degree in computer science from the University of Minnesota, Twin Cities, MN, USA, in 2005.

He is an Associate Professor of Department of Computational Medicine and Bioinformatics and Department of Electrical Engineering and Computer Science at the University of Michigan, Ann Arbor, MI, USA. His research interests include machine learning, data mining, and biomedical informatics. Dr. Ye has served as Senior Program Committee/Area Chair/Program Committee Vice Chair of many conferences including NIPS, ICML, KDD, IJCAI, ICDM, SDM, ACML, and PAKDD. He serves as a PC Co-Chair of SDM 2015. He serves as an Associate Editor for IEEE TRANSACTIONS ON KNOWLEDGE AND DATA ENGINEERING and IEEE TRANSACTIONS ON PATTERN ANALYSIS AND MACHINE INTELLIGENCE, and serves as an Action Editor for Data Mining and Knowledge Discovery. He won the NSF CAREER Award in 2010. His papers have been selected for the outstanding student paper at ICML in 2004, the KDD best research paper honorable mention in 2010, the KDD best research paper nomination in 2011 and 2012, the SDM best research paper runner up in 2013, the KDD best research paper runner up in 2013, and the KDD best student paper award in 2014.